Low-energy electrodynamics of SmB_6

B. Gorshunov
General Physics Institute, Russian Academy of Sciences, Moscow 117942, Russia
and Experimentalphysik V, Universität Augsburg, D-86135 Augsburg, Germany

N. Sluchanko and A. Volkov
General Physics Institute, Russian Academy of Sciences, Moscow 117942, Russia

M. Dressel
Experimentalphysik V, Universität Augsburg, D-86135 Augsburg, Germany
and 1. Physikalisches Institut, Universität Stuttgart, D-70550 Stuttgart, Germany

G. Knebel and A. Loidl
Experimentalphysik V, Universität Augsburg, D-86135 Augsburg, Germany

S. Kunii
Department of Physics, Tohoku University, Sendai 980, Japan
(Received 26 May 1998)

We have performed direct measurements of the low-temperature dynamical conductivity and dielectric permittivity of single crystalline SmB_6 in the spectral range from 0.6 to 4.5 meV, i.e., below the hybridization gap. The obtained results together with the data of Hall-effect and infrared reflection measurements give evidence for a 19-meV energy gap in the density of states and an additional narrow donor-type band lying only 3 meV below the bottom of the upper conduction band. It is shown that at temperatures $5\ \mathrm{K} < T < 20\ \mathrm{K}$ the electrodynamic response and the dc conductivity of SmB_6 are determined by quasifree carriers thermally excited in the conduction band. We evaluate the microscopic parameters of these carriers: the spectral weight, the concentration, the effective mass, the scattering rate, and the mobility. Below 8 K the concentration of carriers in the conduction band freezes out exponentially and finally the electronic properties of SmB_6 are determined by the localized carriers in the narrow band with the typical signature of hopping conductivity. [S0163-1829(99)07603-1]

I. INTRODUCTION

Samarium hexaboride is a typical representative of intermediate valence semiconductors and it may be considered as a prime example of a Kondo insulator.[1–3] The magnetic susceptibility reveals the characteristic features of an intermediate valence compound: a Curie-Weiss-like susceptibility for $T > 100$ K indicative of local-moment behavior and a Pauli spin susceptibility for the lowest temperatures due to a nonmagnetic configuration for $T \to 0$ K. The cusp in the susceptibility close to 80 K can be taken as a rough estimate of the characteristic spin-fluctuation temperature T^*. In Kondo insulators the gap due to the coherent on-site hybridization between the narrow $4f$ states with the band states is expected to be of the same order of magnitude.

Almost three decades after the pioneering investigations of Nickerson *et al.*[4] a large number of detailed and comprehensive studies of SmB_6 have been performed; however, many fundamental properties of SmB_6 such as the electrical transport mechanism are not fully understood. The dc resistivity ρ_{dc} is slightly temperature dependent down to 50 K below where it starts to increase exponentially[5,6] due to the opening of a hybridization gap in the density of states (DOS);[1] there exists a general agreement that the increase between $20\ \mathrm{K} < T < 5$ K can be described by an exponential increase, $\rho_{dc}(T) \propto \exp(-E/2k_BT)$, with a gap[7] $E \approx 5-7$ meV.[8–12] However, there exists significant disagreement about the temperature-dependent conductivity below 5 K. Hopping transport due to localized charge carriers close to the Fermi level and/or thermally activated behavior have been proposed in addition to a residual conductivity.[5,13] The residual conductivity has been interpreted in terms of the Mott minimum conductivity,[10,14] as a Wigner lattice formation,[13] in terms of long-range composition fluctuations,[14] or attributed to surface states which act as a dirty metal in parallel to the intrinsic bulk sample.[12]

A lot of activity has been devoted to determining the value of the low-temperature gap in the DOS spectrum of SmB_6. Measurements of resistivity, Hall effect, tunneling and point-contact spectroscopy, optical transmission and reflection, electron spin resonance, nuclear magnetic resonance relaxation rate, elastic constant, specific heat, and current-voltage characteristics lead to values which can roughly be divided into two groups: small (3–5 meV) and large (10–15 meV) gaps (for reviews see Refs. 1 and 15). Using electron spin resonance[16] some experimental evidence has been provided that the gap opens below 100 K. One of the most straightforward methods to measure a gap in the DOS is provided by the optical spectroscopy. However, in SmB_6 such a task is nontrivial since the small energy scale makes it

difficult to use standard far-infrared techniques. Experiments performed on thin ($d \leqslant 100\ \mu$m) films and layers lead to $E \leqslant 10$ meV,[17] $E \approx 3$ meV,[9] $E \approx 3.7$ meV, or $E \approx 13.7$ meV.[15,18] From the bulk reflectivity measurements[18–20] E was estimated to lie in the range 5–10 meV. The uncertainty is caused by the difficulty of measuring very small transmission or high reflection coefficients of small samples at very low frequencies. In addition, standard Fourier transform spectrometers measure only *one* parameter, transmissivity or reflectivity, and thus have to utilize the Kramers-Kronig relations to evaluate the *two* optical parameters, for instance, the conductivity and dielectric permittivity.[19] In the case of SmB_6, the low-frequency extrapolation of the infrared (IR) reflectivity spectra[19] towards the dc conductivity, necessary for the Kramers-Kronig analysis, leads to numerous mistakes, since the extrapolation does not take into account the low-energy excitations reported in this article.

The aim of the present investigation was to apply a submillimeter (submm) quasioptical spectroscopic method for performing the first *direct* measurements of the spectra of both optical parameters, the real parts of the dynamical conductivity $\sigma(\nu)$ and of the dielectric permittivity $\varepsilon(\nu)$, of SmB_6 single crystal at photon energies 0.6–4.5 meV, below the hybridization-gap energy, and to study the electronic properties of SmB_6 by analyzing the obtained submm spectra together with the dc conductivity and Hall data measured for the same sample and with the high-frequency infrared spectra. Performing transmission experiments allows us to calculate the conductivity and permittivity directly.

II. EXPERIMENTAL TECHNIQUES

The single crystals of SmB_6 were grown by a floating zone method. The high quality is characterized by a large ratio $\rho(60\text{ mK})/\rho(300\text{ K}) \approx 4 \times 10^6$. The Hall voltage and the dc resistivity were measured by standard four-probe method. The measurement of the Hall coefficient was performed in the linear range of the Hall voltage versus magnetic field. We plan to give a full discussion of the field-dependent Hall coefficient and low-temperature magnetoresistance up to 14 T elsewhere.[21]

For the submm transmissivity measurements a disk of diameter ≈ 6 mm, cut out of the same bulk piece of the SmB_6 single crystal on which the dc measurements were performed, was polished down to a thickness $d = 28\ \mu$m with planes parallel to better than $\pm 1\ \mu$m. The investigations were performed on a coherent-source spectrometer using a Mach-Zehnder arrangement.[22] From the *two* experimentally accessible independent parameters, the transmission coefficient $Tr(\nu)$ and the phase shift $\varphi(\nu)$ of the radiation passed through the plane-parallel sample, the spectra of dynamical conductivity $\sigma(\nu)$ and dielectric permittivity $\varepsilon(\nu)$ can be calculated *directly* by Fresnel's equations without utilizing the Kramers-Kronig relation.[23]

III. RESULTS AND ANALYSIS

Figure 1 shows the dc conductivity $\sigma_{dc}(T)$ of our sample in the temperature range 60 mK–300 K plotted in different ways in order to stress the various temperature dependences.

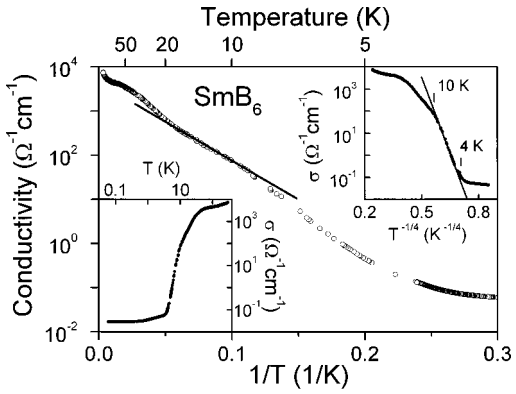

FIG. 1. Arrhenius plot of the dc conductivity of SmB_6. The line corresponds to $\sigma_{dc} \propto \exp[(3.5\text{ meV})/k_B T]$. The inset in the lower left corner shows the overall behavior of $\sigma_{dc}(T)$ in a double logarithmic way. The inset in the upper right corner shows the conductivity as a function of $T^{-1/4}$.

Main features are in accordance with the literature data. Between 8 and 25 K the conductivity can be described by $\sigma_{dc}(T) \propto \exp(E_d/k_B T)$ with $E_d \approx 3.5$ meV. We found that $\sigma_{dc}(T) \propto \exp(T_0/T^{1/4})$ with $T_0 = 53$ K fits our data best in the range from 4 K to approximately 10 K. For $T \approx 1$ K and lower, $\sigma_{dc}(T)$ becomes basically temperature independent.

The original submm spectra of transmissivity and phase shift (divided by the frequency in wave numbers) are presented in Fig. 2. It is seen that the sample becomes more transparent at lower temperatures and that at $T = 3$ K periodic

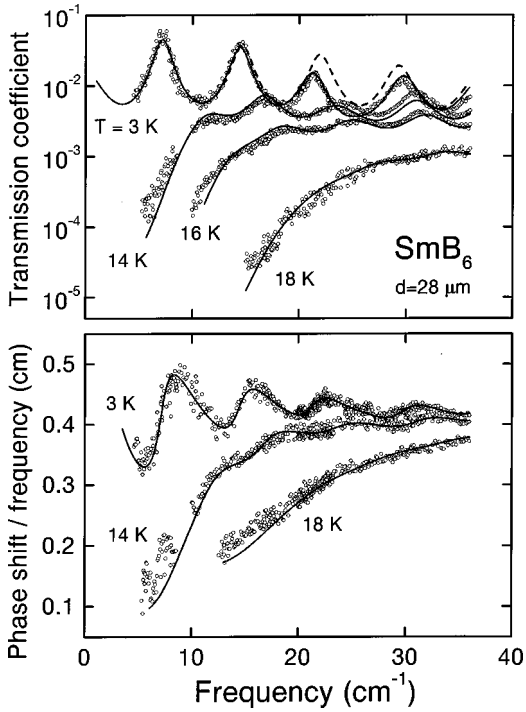

FIG. 2. Submillimeter spectra of the transmission coefficient and the phase shift of the radiation (divided by ν) passed through the 28-μm-thick SmB_6 plane-parallel sample, at selected temperatures. Solid lines show the results of the least-squares fit of the submm spectra of conductivity and permittivity using Eq. (1). The dashed line corresponds to the result when the oscillator terms ε_{osc} and σ_{osc} are not included.

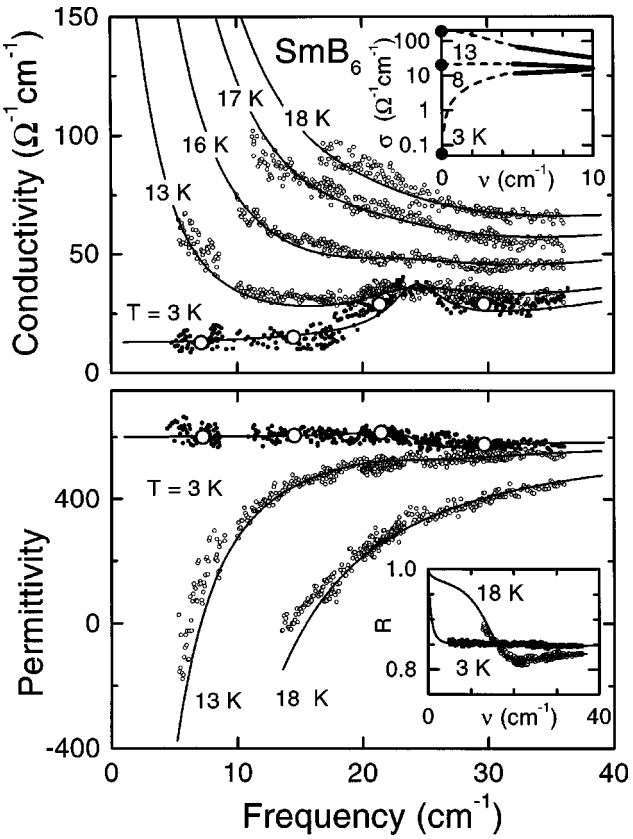

FIG. 3. Spectra of the conductivity and the dielectric permittivity of SmB_6 at selected temperatures. The solid lines show a fit by Eq. (1). The large open dots in the 3-K spectra are evaluated using the interference maxima in the transmission spectrum. The inset in the upper panel compares these data with the dc conductivity (large solid dots). The interpolation (dashed lines) is done by a Drude term, by a constant value, and by $\sigma(\nu)\propto\nu$ for 13, 8, and 3 K, respectively. The inset of the lower panel shows the spectra of the bulk reflection coefficient calculated from the measured conductivity and permittivity spectra. The solid lines correspond to the calculations by Eq. (1).

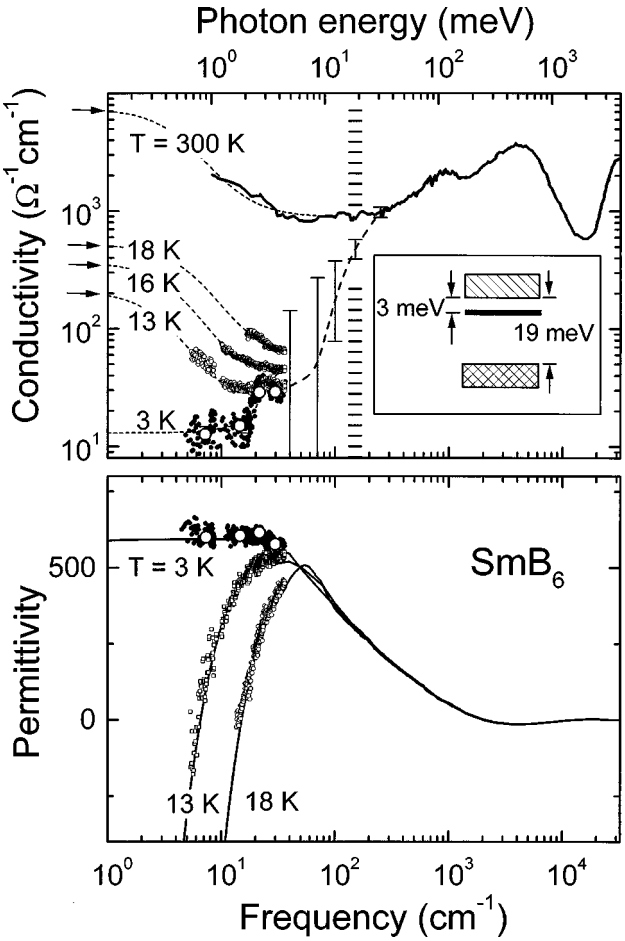

FIG. 4. Frequency-dependent conductivity (upper panel) and dielectric permittivity (lower panel) of SmB_6 at different temperatures. The small dots correspond to the submm data; the arrows to the dc conductivity. The solid lines shown are obtained by the Kramers-Kronig analysis of the reflectivity spectra (data from Ref. 18 corrected to the submm reflectivity). The long-dashed line interpolating the 3-K data sets is a guide the eye. The error bars give the upper and lower boundary of the IR conductivity obtained by the Kramers-Kronig analysis of the 3-K reflectivity spectrum assuming a 0.5% uncertainty. The dashed lines are the results calculated by Eq. (1). The 300-K conductivity spectrum is taken from Ref. 18. The shaded area corresponds to the energy gap value (19 $\pm$2) meV. The inset in the upper frame gives a simplified view of the band scheme of SmB_6.

maxima are well pronounced in the transmissivity (and phase) spectra. These maxima are interferometric and appear due to multiple reflection of the radiation on the plane-parallel faces of the sample when its optical thickness *nd* equals a multiple of half the wavelength.[23] In our case interference effects are observed even in a very thin (28 μm) sample due to its large low-temperature refractive index $n(T=3\text{ K})\approx 24.5$. The presence of the interference fringes (maxima) in the transmission spectrum allows us to evaluate *both* optical parameters of the sample without additional measuring of the phase, since the height of the transmissivity maxima is determined by the extinction coefficient k and the period of the oscillations by the refractive coefficient n.[23] This is seen in Fig. 3 where the conductivity $\sigma(\nu)$ and permittivity $\varepsilon(\nu)$ are displayed calculated from $Tr(\nu)$ and $\varphi(\nu)$ for each frequency. These values agree well with the results obtained from the interferometric maxima in the transmissivity and presented by open dots in the 3-K spectra. Two characteristic types of behavior can be seen in the spectra of Fig. 3. First, there is a Drude-like dispersion of $\sigma(\nu)$ and $\varepsilon(\nu)$ at high temperatures ($T>13$ K) typical for the response of free charge carriers:[24] the conductivity decreases and the permittivity increases towards high frequencies. Second, at 3 K the $\varepsilon(\nu)$ spectrum becomes dispersionless as is characteristic for a dielectric material, with a value of the dielectric permittivity $\varepsilon(0)\approx 600\pm 20$ (refractive coefficient $n=\varepsilon^{1/2}=24.5$ since $k\ll n$), significantly smaller than $\varepsilon(0)\approx 1500$ previously estimated in Ref. 19. The absorption peak at about 24 cm^{-1} in the 3-K conductivity spectrum of Fig. 3 is also seen with the correspondent step in $\varepsilon(\nu)$. The bulk reflectivity spectra *calculated* on the basis of our data (inset in the lower panel of Fig. 3) show a well pronounced plasma edge at 18 K which flattens out at 3 K.

Figure 4 presents the frequency-dependent conductivity and permittivity of SmB_6 in a broad range. The infrared conductivity was obtained by the Kramers-Kronig analysis of the reflectivity spectrum measured for the sample from the same batch.[18,21] At lower temperatures we used the reflectiv-

ity calculated from our submm measurements of σ and ε to correct the far-infrared reflectivity. We found that for $\nu < 200\ \mathrm{cm}^{-1}$ the low-temperature IR reflectivity of SmB_6 is mainly determined by the large permittivity and is only slightly dependent on the conductivity. This leads to a large uncertainty in the conductivity values as obtained by the Kramers-Kronig analysis. The error bars in Fig. 4 show the uncertainty of the 3-K conductivity at around 100 cm^{-1} which leads to only a $\pm 0.5\%$ deviation in the reflectivity. The dashed line between the two data sets is a guide to the eye.

Already at this point we would like to draw attention to the inset of the upper frame of Fig. 3. The conductivity in the submm range decreases by only one order of magnitude on cooling from 13 to 3 K. In the same temperature range, σ_{dc} drops by more than four orders of magnitude. Close to 8 K the low-frequency behavior changes from free-carrier to localized-carrier transport. Thus below 8 K the difference between the submm and the dc conductivity (indicated by the dashed line at 3 K) is of about two orders of magnitude and is, most probably, due to hopping processes at low frequencies.

We fitted the conductivity and permittivity spectra using the following expressions:

$$\sigma = \sigma_{\mathrm{Drude}} + \sigma_{\mathrm{osc}} + \sigma_{\mathrm{IRosc}} + \sigma_{\mathrm{min}},$$
$$\varepsilon = \varepsilon_{\mathrm{Drude}} + \varepsilon_{\mathrm{osc}} + \varepsilon_{\mathrm{IRosc}} + \varepsilon_{\mathrm{inf}}, \tag{1}$$

where σ_{Drude} and $\varepsilon_{\mathrm{Drude}}$ describe the free-carrier response, σ_{osc} and $\varepsilon_{\mathrm{osc}}$ the 24-cm^{-1} peak, σ_{IRosc} and $\varepsilon_{\mathrm{IRosc}}$ the IR conductivity and permittivity, and $\varepsilon_{\mathrm{inf}}$ is the high-frequency contribution to the dielectric permittivity. For a complete description of the conductivity spectra an additional parameter σ_{min} had to be introduced in the form of a frequency-independent (throughout the submm range) component which we call the minimum-conductivity term.

The free-carrier response is governed by the expressions coming from the Drude conductivity model:[24]

$$\sigma_{\mathrm{Drude}}(\nu) = \sigma_0 \gamma^2 (\gamma^2 + \nu^2)^{-1},$$
$$\varepsilon_{\mathrm{Drude}}(\nu) = -2\sigma_0 \gamma (\gamma^2 + \nu^2)^{-1}, \tag{2}$$

where $\gamma = 1/2\pi\tau$ is the damping rate and $\sigma_0 = \nu_{\mathrm{pl}}^2/2\gamma = Ne\mu$ is the conductivity for $\nu = 0$. Here ν_{pl} is the plasma frequency and $\mu = e\tau/m^*$ is the mobility. The square of the plasma frequency (called the spectral weight) is related to the ratio of density N and effective mass m^* of the charge carrier, $\nu_{\mathrm{pl}}^2 = Ne^2/\pi m^*$. The oscillator terms in Eq. (1) are commonly given by

$$\sigma_{\mathrm{osc}}(\nu) = 0.5 f \nu^2 \gamma_{\mathrm{osc}} [(\nu_0^2 - \nu)^2 + \gamma_{\mathrm{osc}}^2 \nu^2]^{-1},$$
$$\varepsilon_{\mathrm{osc}}(\nu) = f(\nu_0^2 - \nu^2)[(\nu_0^2 - \nu)^2 + \gamma_{\mathrm{osc}}^2 \nu^2]^{-1}, \tag{3}$$

where ν_0 is the eigenfrequency, γ_{osc} indicates the oscillator damping, $f = \Delta\varepsilon \nu_0^2$ is the oscillator strength (corresponding to the spectral weight), and $\Delta\varepsilon$ is the dielectric contribution of this term. The fits are shown by solid lines in Figs. 2–4; the temperature variation of the parameters is given in Figs. 5 and 6. The IR oscillator ($\nu_0 = 2000\ \mathrm{cm}^{-1}$, $\Delta\varepsilon = 370$, $\gamma = 7100\ \mathrm{cm}^{-1}$) is determined by fitting the 3-K data, where no Drude free-carrier contribution is present; its parameters are kept unchanged at higher temperatures.

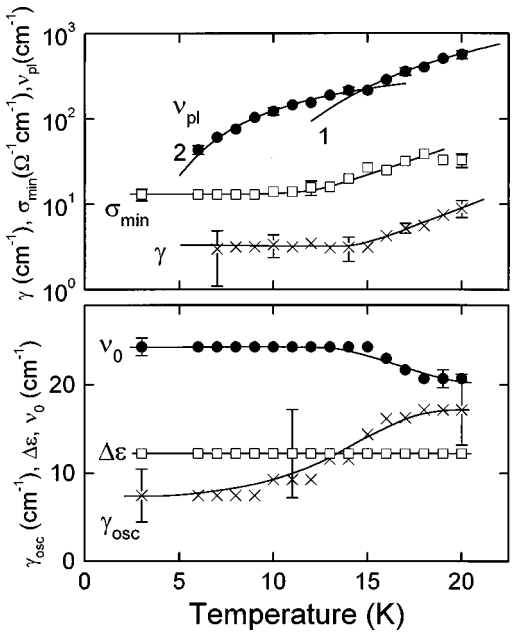

FIG. 5. The upper panel shows the temperature dependences of the plasma frequency ν_{pl} of free charge carriers of SmB_6, of the scattering rate γ, and of the basement conductivity σ_b as obtained by a fit using the model of Eq. (1). The solid line (1) corresponds to the activated behavior $\nu_{\mathrm{pl}} \propto \exp(-E_g/4k_BT)$ with $E_g = 19$ meV; the line (2) indicates $\nu_{\mathrm{pl}} \propto \exp(-E_d/2k_BT)$ with $E_d = 3$ meV. The dashed lines are guides to the eye. The parameters of the oscillator found in the submm range have a temperature dependence as displayed in the lower panel: ν_0 is the eigenfrequency, $\Delta\varepsilon$ is the dielectric contribution, and γ is the damping constant. The dashed lines guide the eye.

The upper panel of Fig. 5 shows the temperature dependence of the Drude parameters which describe the free carriers above approximately 8 K, namely, the plasma frequency and the relaxation rate, together, and the minimum

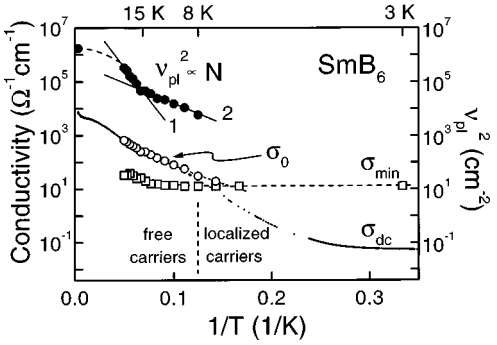

FIG. 6. Temperature dependence of the squared plasma frequency ν_{pl}^2 (solid dots) and of the Drude conductivity σ_0 (open dots) of SmB_6. The straight line (1) corresponds to $\nu_{\mathrm{pl}}^2 \propto \exp(-E_g/2k_BT)$ with $E_g = 19$ meV; the second line (2) is given by $\nu_{\mathrm{pl}}^2 \propto \exp[(3\ \mathrm{meV})/k_BT]$. The small solid dots in the lower part correspond to the dc conductivity. The open squares indicate the minimum-conductivity term. The dashed lines are guides to the eye.

conductivity. The lower panel gives the parameters determined from the fit to the oscillator close to 24 cm^{-1} which significantly contributes to the conductivity in this frequency range at low temperatures.

IV. DISCUSSION

From Figs. 3 and 4 it is seen that for $T>8$ K the submm electrodynamic response of SmB_6 resembles a free-carrier behavior. The measured dc conductivity agrees with σ_0 obtained by fitting the submm spectra of $\varepsilon(\nu)$ and $\sigma(\nu)$ using the Drude expressions (Figs. 4 and 6), implying that the low-energy transport is fully determined by free carriers in the conduction band. Using Eq. (1) allows us to determine $\gamma(T)$ and $\nu_{pl}(T)$ of the correspondent free charge carriers, as plotted in Figs. 5 and 6. The temperature dependence of the scattering rate γ of these carriers (Fig. 5) shows decreasing below 20 K indicating phonon-assisted scattering; below 15 K defect scattering becomes dominant with $\gamma=$const. The spectral weight $\nu_{pl}^2(T)$ directly corresponds to the number of free carriers in the conduction band: $N=\nu_{pl}^2 m^* \pi/e^2$. Here we assume that m^* is temperature independent, an assumption that should be valid for $T \ll T^*$. Figure 6 shows $\nu_{pl}^2(T)$ versus $1/T$. In terms of a semiconductor phenomenology we can analyze the carrier density between approximately 30 and 8 K assuming two regimes governed by different activation energies. Using $\nu_{pl}^2 \propto \exp(-E_g/2k_BT)$ for $10\ \mathrm{K}<T<15$ K, we find an activation energy of $E_g=19$ meV (solid line 1) which corresponds to the hybridization gap as observed in the optical spectroscopy (see dashed area in the upper panel of Fig. 4). We do not want to speculate whether the gap develops in a mean-field behavior, or whether it is temperature independent and just fills in as the temperature rises; but there are indications that the latter scenario takes place. For lower temperatures we find a much smaller activation energy (solid line 2) which most likely indicates a narrow donor-type band[5,9,10] inside the gap. Assuming the Fermi energy lying within this band and thus $\nu_{pl}^2 \propto \exp(-E_d/k_BT)$, we obtain the narrow band located $E_d=3$ meV below the bottom of the conduction band. At exactly the frequency corresponding to E_d we observe a peak in the sub-mm spectrum which therefore can be associated with direct excitations of charge carriers from the narrow band to the conduction band. We then can use the oscillator fit with the parameters shown in Fig. 5 and estimate the plasma frequency and scattering rate of the carriers in the band $\nu_{pl}=\Delta\varepsilon^{1/2}\nu_0 \approx 90\ \mathrm{cm}^{-1}$ and $\gamma=\nu_{pl}^2/2\sigma_0 \approx 70\ \mathrm{cm}^{-1}$. We cannot really decide whether the in-gap narrow band is connected with imperfections or has intrinsic origin; however, we have observed the 24-cm^{-1} structure in another SmB_6 sample with much higher impurity concentration of 10^{15} to 10^{16} cm^{-3}.[21] Ohta *et al.*[15] also report indications of two gap values and suggest impurities or defects as the origin of the sublevels.

In the limited range $8\ \mathrm{K}<T<15$ K, the temperature dependence of the carrier density as determined from the plasma frequency corresponds well to $\sigma_{dc}(T)$, which is also included in Fig. 6 (open circles). Above 15 K the temperature dependence of the scattering rate cannot be neglected in the description of $\sigma_{dc}(T)$ as seen by the deviation of $\nu_{pl}^2(T) \propto N(T)$ from $\sigma_{dc}(T)$. Significant deviations also appear below 8 K, characterizing the transition from a free-carrier behavior to localization of carriers (inset of Fig. 3). As pointed out earlier, at 8 K the optical conductivity is frequency independent up to 30 cm^{-1} (without considering the 24-cm^{-1} peak) and at lower temperatures the low-frequency response must be dominated by hopping conduction which is characterized by a temperature dependence as $\sigma_{dc}(T) \propto \exp(T_0/T^{1/4})$ and a frequency dependence $\sigma(\nu) \propto \nu^s$ with $s \approx 0.8$.[25] Preliminary experiments in the MHz and GHz range support these predictions.[21] However, the frequency exponent s itself is frequency dependent, reaching low values at high frequencies and yielding a saturation of the conductivity close to far-infrared (FIR) frequencies[26] as indeed is observed here. The fit of the temperature dependence by the model of variable-range hopping[26] yields a reasonable value of $T_0=54$ K. At low temperatures, this high-frequency saturation obviously corresponds to the value σ_{min} which has been determined in our fits of the submm data. We may speculate that this value of σ_{min} gives the value of the minimum metallic conductivity which has been introduced by Mott[14] many years ago. Concerning the temperature dependence, it separates metallic and hopping transport; in terms of frequency it is constant just at this transition temperature of 8 K, indicating that the last free carriers become localized below this temperature. The value of the minimum conductivity in SmB_6 has been calculated[10] as 5.7 $(\Omega\ \mathrm{cm})^{-1}$, a value remarkably close to the value we found (Fig. 6).

TABLE I. Parameters of the charge carriers in SmB_6 calculated on the basis of the measured Hall constant R_H and on the relaxation frequency γ and plasma frequency ν_{pl} obtained from the submillimeter conductivity and permittivity spectra.

T (K)	R_H (cm^3/C)	γ (cm^{-1})	μ_H ($cm^2\ V^{-1}\ s^{-1}$)	N (10^{19} cm^{-3})	m^*/m_0
14	−0.35	3	80	1.8	110
16	−0.19	4.3	66	3.2	94
18	−0.117	5.5	52	5.7	94

In Fig. 4 the features of a narrow-gap semiconductor behavior of SmB_6 are demonstrated by the spectra of $\varepsilon(\nu)$ and $\sigma(\nu)$ over a wide frequency range, nicely showing the fundamental absorption edge at 10–20 meV which leads to the large low-temperature permittivity $\varepsilon(0)=600$. The shaded area marks the value of the energy gap estimated from our data on the temperature dependence of the squared plasma frequency as $E_g=19\pm2$ meV under the assumption that the Fermi energy is in the middle of the gap. A comparison with the reflectivity measurements of Travaglini and Wachter[19] shows some quantitative differences, although the main features of the conductivity spectrum and the important conclusions remain valid. The IR maximum is reported at 1000 cm^{-1}, and the optical gap at 30 cm^{-1}; the latter value is influenced by the extrapolation to the dc conductivity.[1] We find that for temperatures $T<5$ K the Drude-like dispersion of $\varepsilon(\nu)$ and $\sigma(\nu)$ has disappeared (according to an exponential decrease of the carrier concentration $N \propto \nu_{pl}^2$ in the conduction band) and the submm response is dominated by a nearly temperature-independent conductivity term $\sigma_{min}=$const which indicates carriers moving in the narrow band

as quasifree particles with $\gamma \gg \nu \approx 15\ \mathrm{cm}^{-1}$ (Hagen-Rubens limit of the free-carrier response). At approximately 8 K we observe a temperature-independent conductivity from dc up to 35 cm^{-1}.

Assuming only electrons participating in the transport, our Hall data together with γ and ν_{pl} allow us to evaluate the mobility and the effective mass of the carriers (Table I). The values of the Hall mobility μ_H agree with Refs. 7 and 10, however, $m^* \approx 100 m_0$ is considerably smaller than the estimate $m^*/m_0 = 500-1500$ made in Ref. 19. Nevertheless we find a narrow peak in the density of states at the bottom of the conduction band and correlation effects are important.

The large discrepancy in the gap values E reported in the literature ranging from 2 to 16 meV can now be explained consistently. The gap values of only a few meV detected in various experiments[9,15,17,27–29] correspond to the energy difference between the bottom of the conduction band and the peak in the DOS (narrow band) *inside* the hybridization gap. The latter one has a considerably larger width of 19 meV and corresponds to features reported in the range 14–16 meV.[15,30] The two activation mechanisms agree well with the temperature dependence of the Hall constant R_H;[9,10] in the temperature range $50\ \mathrm{K} < T < 15\ \mathrm{K}$ an exponential behavior with an energy $E_g/2$ was found which decreases to 3 meV for $15\ \mathrm{K} < T < 6\ \mathrm{K}$. Below 6 K considerable deviations from the activationlike behavior of R_H are observed in Refs. 9 and 10 which may be due to localization effects, as discussed above. It is important to note that the hybridization gap corresponds to the $E_g = 19$-meV gap. Grewe and Steglich[31] and Jarrell[32] have calculated the hybridization gap and found that $E_g \approx 2T^*$. In the case of SmB_6 this would yield a gap value of $160\ \mathrm{K} \approx 14$ meV which is close to the experimentally observed gap energies. The observed effective mass $m^* \approx 100 m_0$ also agrees well with this picture. Concomitantly a spin gap of the same size is expected[32] and indeed in neutron scattering results a spin gap of 14 meV has been detected[33] and has the correct order of magnitude for a system with a characteristic temperature $2T^* \approx 100$ K.

V. CONCLUSIONS

We have performed direct measurements of the dynamical conductivity and dielectric permittivity of single crystalline samarium hexaboride in the frequency range from 5 to 36 cm^{-1} at low temperatures. Above 5 K the electrodynamical properties and the dc conductivity of SmB_6 are determined by quasifree electrons; their concentration changes exponentially with an activation energy $E_g/2$ above 15 K and $E_d = 3$ meV below 15 K. This implies a gap of $E_g = 19$ meV in the SmB_6 density of states and an additional narrow donor-type band lying 3 meV in the gap. The absorption peak discovered at 24 cm^{-1} is connected to the direct photoexcitation of electrons from the narrow band to the upper conduction band. The large value of effective mass $m^* \approx 100 m_0$ indicates the importance of correlation effects in the enhanced density of states at the bottom of the conduction band. At very low temperatures ($T < 5$ K) the contribution of free electrons in the conduction band decreases and the submm conductivity of SmB_6 is nearly frequency independent; we attribute this to the charge carriers within the narrow band. Hopping between localized states governs the electrodynamic properties in the low-frequency regime down to dc.

ACKNOWLEDGMENTS

We acknowledge support by the Russian Foundation for Basic Research Grants No. 97-02-17645 and 96-02-17350. The work at Augsburg was supported by the BMBF under Contract No. EKM 13N6917. The German-Russian collaboration was supported by the Deutsche Forschungsgemeinschaft and the Russian Foundation for Basic Research. The crystal growth was supported by the Ministry of Education, Science and Culture of Japan.

[1] P. Wachter, in *Handbook on the Physics and Chemistry of Rare Earths*, edited by K. A. Gschneider, Jr. and L. Eyring (North-Holland, Amsterdam, 1994), Vol. 19, p. 177, and references therein.

[2] G. Aeppli and Z. Fisk, Comments Condens. Matter Phys. **16**, 155 (1992).

[3] T. Kasuya, Europhys. Lett. **26**, 277 (1994); **26**, 283 (1994).

[4] J. C. Nickerson, R. B. White, K. N. Lee, R. Bachmann, T. H. Geballe, and G. W. Hull, Jr., Phys. Rev. B **3**, 2030 (1971).

[5] I. Bat'ko, P. Farkašovský, and K. Flachbart, Solid State Commun. **88**, 405 (1993).

[6] T. Kasuya, M. Kasaya, T. Takegahara, T. Fujita, T. Goto, A. Tamaki, M. Takigawa, and H. Yasuoka, J. Magn. Magn. Mater. **31-34**, 447 (1983).

[7] Throughout the paper, we denote the literature values of the full gap by E. The hybridization gap determined by our experiments is called E_g. The energy difference between the narrow band and the conduction band is labeled by E_d.

[8] J. Roman, V. Pavlík, K. Flachbart, T. Herrmannsdörfer, S. Rehmann, E. S. Konovalowa, and Yu. B. Paderno, Physica B **230-232**, 715 (1997).

[9] S. von Molnar, T. Theis, A. Benoit, A. Briggs, J. Flouquet, J. Ravex, and Z. Fisk, in *Valence Instabilities*, edited by P. Wachter and H. Boppart (North-Holland, Amsterdam, 1982), p. 389.

[10] J. W. Allen, B. Batlogg, and P. Wachter, Phys. Rev. B **20**, 4807 (1979).

[11] J. C. Cooley, M. C. Aronson, A. Lacerda, P. C. Canfield, Z. Fisk, and R. P. Guertin, Physica B **206&207**, 377 (1995).

[12] A. Kebede, M. C. Aronson, C. M. Buford, P. C. Canfield, Jin Hyung Cho, B. R. Coles, J. C. Cooley, J. Y. Coulter, Z. Fisk, J. D. Goettee, W. L. Hults, A. Lacerda, T. D. McLendon, P. Tiwari, and J. L. Smith, Physica B **223&224**, 256 (1996).

[13] T. Kasuya, K. Takegahara, T. Fujita, T. Tanaka, and E. Bannai, J. Phys. (Paris), Colloq. **40**, C5-308 (1979).

[14] N. F. Mott, in *Valence Instabilities*, edited by P. Wachter and H. Boppart (North-Holland, Amsterdam, 1982), pp. 397 and 403.

[15] H. Ohta, R. Tanaka, M. Motokawa, S. Kunii, and T. Kasuya, J. Phys. Soc. Jpn. **60**, 1361 (1991), and references therein.

[16] T. S. Al'tshuler, V. N. Mironov, G. G. Khaliullin, and D. I. Khomskii, Pis'ma Zh Eksp. Teor. Fiz. **40**, 28 (1984) [JETP Lett. **40**, 754 (1984)].

[17] B. Battlog, P. H. Schmidt, and J. M. Rowell, in *Valence Fluctuations in Solids*, edited by L. M. Falicov, W. Handke, and M. B. Maple (North-Holland, Amsterdam, 1981), p. 267.
[18] T. Nanba, H. Otha, M. Motokawa, S. Kimura, S. Kunii, and T. Kasuya, Physica B **186-188**, 440 (1993).
[19] G. Travaglini and P. Wachter, Phys. Rev. B **29**, 893 (1984).
[20] S. Kimura, T. Nanba, S. Kunii, and T. Kasuya, Phys. Rev. B **50**, 1406 (1994).
[21] M. Dressel *et al.* (unpublished).
[22] G. Kozlov and A. A. Volkov, in *Millimeter and Submillimeter Wave Spectroscopy of Solids*, edited by G. Grüner (Springer, Berlin, 1998).
[23] M. Born and E. Wolf, *Principles of Optics*, 6th ed. (Pergamon, Oxford, 1980).
[24] A. V. Sokolov, *Optical Properties of Metals* (Blackie & Sons, London, 1967).
[25] A. A. Gogolin, Phys. Rep. **86**, 1 (1982); H. Böttger and V. V. Bryksin, Phys. Status Solidi B **78**, 415 (1976); **113**, 9 (1982).
[26] N. F. Mott and E. A. Davis, *Electronic Processes in Non-Crystalline Materials*, 2nd ed. (Clarendon, Oxford, 1979); S. R. Elliott, Adv. Phys. **36**, 135 (1987).
[27] B. Batlogg, Phys. Rev. B **23**, 1827 (1981).
[28] I. Frankowski and P. Wachter, Solid State Commun. **41**, 577 (1982).
[29] G. Güntherodt *et al.*, in *Valence Instabilities*, edited by P. Wachter and H. Boppart (North-Holland, Amsterdam, 1982), p. 313.
[30] S. Kunii, J. Magn. Magn. Mater. **63&64**, 673 (1988).
[31] N. Grewe and F. Steglich, in *Handbook on the Physics and Chemistry of Rare Earths*, edited by K. A. Gschneider, Jr. and L. Eyring (North-Holland, Amsterdam, 1991), Vol. 14, p. 343.
[32] M. Jarrell, Phys. Rev. B **51**, 7429 (1995).
[33] P. A. Alekseev, J.-M. Mignod, J. Rossat-Mignod, V. N. Lazukov, and I. P. Sadikov, Physica B **186-188**, 384 (1993); P. A. Alekseev, J.-M. Mignod, J. Rossat-Mignod, V. N. Lazukov, I. P. Sadikov, E. S. Kanovalova, and Yu. B. Paderno, J. Phys.: Condens. Matter **7**, 289 (1995).